Journal of Colloid and Interface Science 720 (2026) 140629

Contents lists available at ScienceDirect

Journal of Colloid And Interface Science

journal homepage: www.elsevier.com/locate/jcis

Transfer of molecular handedness to complex systems shaped by non chiral polyamines

Francesca Ceccacci [a,1], Beatrice Simonis [a,1], Serena Ponte [a,b], Marco Mazzonna [c], Adriana Pietropaolo [d,**], Stefano Borocci [c,e,*], Giovanna Mancini [c,*]

[a] CNR-ISB, Istituto per i Sistemi Biologici, Sede Secondaria di Roma-Meccanismi di Reazione c/o Dipartimento di Chimica, Sapienza Università di Roma, P.le A. Moro 5, Rome, Italy
[b] Dipartimento di Chimica, Sapienza Università di Roma, P.le A. Moro 5, Rome, Italy
[c] CNR-ISB, Istituto per i Sistemi Biologici, Area territoriale di Ricerca di Roma 1, SP35d 9, 00010 Montelibretti, Rome, Italy
[d] Dipartimento di Scienze della Salute, Università di Catanzaro, Catanzaro, Italy
[e] Dipartimento per l'Innovazione nei sistemi Biologici, Agroalimentari e Forestali (DIBAF), Università della Tuscia, L.go dell'Università, s.n.c, Viterbo 01100, Italy

GRAPHICAL ABSTRACT

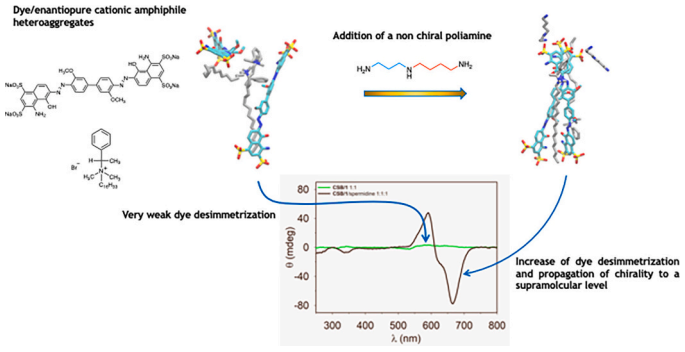

ARTICLE INFO

Keywords:
Supramolecular chirality
Chiral surfactant
Dye
Circular dichroism
Deracemization
Metadynamics

ABSTRACT

A remarkable hallmark of Nature is its inherent lack of left-right symmetry across all scales of size and complexity, from elementary particles up to macroscopic systems such as animals, plants and flowers.

One of the questions raised by Nature propensity to favour one handedness over the other concerns the correlation of dissymmetry across different levels of complexity.

Because Nature's complexity arises through self-assembling of molecules and macromolecules into organisms whose structure, symmetry features and functions are controlled by non-covalent interactions, we employ a dye–surfactant assembly as a model system. Using circular dichroism spectroscopy combined with molecular dynamics simulations we show that the chirality of complex systems can be modulated by non-chiral molecules

* Corresponding authors at: CNR-ISB, Istituto per i Sistemi Biologici, Area territoriale di Ricerca di Roma 1, SP35d 9, 00010 Montelibretti, Rome, Italy.
** Corresponding author.
E-mail addresses: apietropaolo@unicz.it (A. Pietropaolo), borocci@unitus.it (S. Borocci), giovanna.mancini@cnr.it (G. Mancini).
[1] These authors contributed equally.

https://doi.org/10.1016/j.jcis.2026.140629
Received 29 January 2026; Received in revised form 15 April 2026; Accepted 27 April 2026
Available online 30 April 2026

such as polyamines. This finding provides a different framework for exploring the transmission of chirality, suggesting that non-chiral metabolites may also contribute to chiral shaping.

1. Introduction

One of the unresolved issues regarding the chiral homogeneity of Nature concerns the propagation of symmetry breaking across different levels of complexity. Several investigations have indicated that the handedness of chiral systems at the macroscopic levels is controlled by that of biomolecules [1–13], however a comprehensive description of the propagation of chirality from one level of complexity to the next has yet to be fully elucidated.

Nano-sized self-assemblies at a low hierarchical level of complexity are optimal tools for investigating the transcription, evolution, and amplification of chirality from one level to next hierarchical level of complexity. The contribution of hydrogen bond, metal-ligand coordination, electrostatic, π-π, cation-π interactions in the transcription of chirality were clearly evidenced [14–24]. Some reports also pointed out the role of hydrophobic interactions, though these might be more elusive [14,23–30]. In particular it was shown that the balance between electrostatic and hydrophobic interactions can tune the transcription of the chiral information from a chiral cationic surfactant to the assemblies it forms with an anionic dye [28–30].

It is known that aggregation of surfactants and dyes of opposite charge occurs at surfactant concentrations far below the critical micelle concentration of the surfactant, inducing relevant changes in the UV–vis spectrum of the dye [31,32]. However, the organization of these aggregates is still object of investigation. We had observed that the interaction of a chiral cationic surfactant with a dye such as Congo Red or Chicago Sky Blue (**CSB**) can induce the occurrence of bands in the circular dichroism (CD) spectrum of the dye/surfactant aggregate, within the region of absorbance of the dye. Such CD bands may originate from the enantiomeric excess generated by the deracemization of a chiral conformation of the dye itself (*i.e.* at a molecular level) and/or by the deracemization of a chiral arrangement of dye molecules (*i.e.* at a supramolecular level), any deracemization being induced by the chiral surfactant [28–30].

For the sake of clarity, here we refer to enantiomers, focusing exclusively on dye molecules. However, irrespective of the nature of the enantiomeric excess, this is induced by the chiral surfactant through diastereomeric interactions.

In this study, we investigated assemblies formed by **CSB** and the chiral enantiopure cationic surfactant (*S*)-*N*,*N*-dimethyl-N-(1-phenylethyl)-esadecan-1-ammonium bromide (**1**) at a 1:1 ratio, focusing on their chiral response to the presence of non-chiral polyamines such as 1,3-diaminopropane, putrescine, cadaverine, norspermidine, spermidine and spermine (Chart 1). Further, as a blank experiment, we explored, the effect of *n*-propylamine at different ratios to simulate the number of amine functions of the polyamines.

Under the experimental conditions the amine groups of polyamines are protonated (the pH of aqueous solution being 6.7) and can interact with the sulfonate groups of the dye through electrostatic interactions, as well as with the aromatic residues of both the dye and the surfactant *via* cationic-π interactions, thus influencing the organization and reciprocal arrangement of the components of **CSB**/**1** assemblies. The different molecular structure and electrostatic potential of polyamines may affect the interaction with the dye/surfactant assembly and the supramolecular organization as well. To identify the molecular interactions responsible for the chiral bias in the final assemblies, we complemented CD experiments with molecular dynamics simulations.

Finally, we verified the formation of **CSB**/**1** large assemblies using both NMR and transmission electron microscopy (TEM).

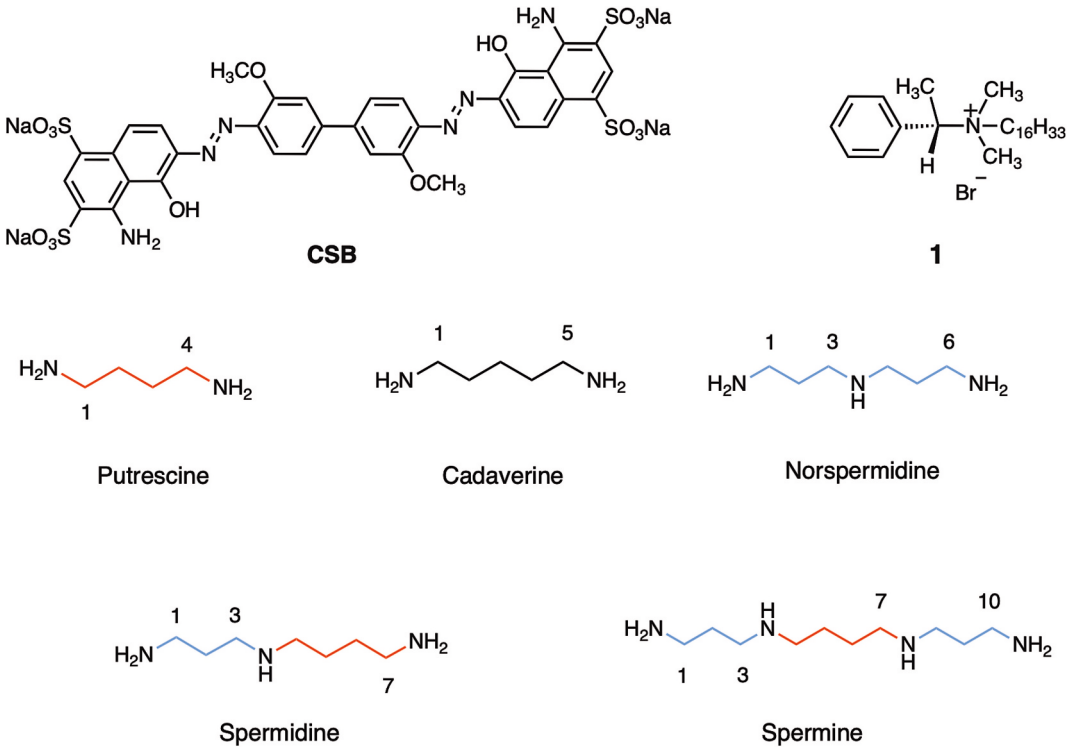

Chart 1. Assembly components.

2. Results and discussion

2.1. CD response of dye/surfactant assemblies

Significant results of the investigation concern the UV–vis and CD spectra of **CSB/1** aggregates including spermidine, norspermidine or spermine (Fig. 1). The presence of any of these polyamines induces a decrease in the absorption band at 600 nm in the UV–vis spectrum of the dye/surfactant aggregate. In the CD spectrum, the weak positive band of the dye/surfactant aggregate at 590 nm in the absence of polyamine becomes more intense in the presence of norspermidine and, interestingly, in the presence of spermidine and spermine is replaced by an intense negative exciton couplet centered at ~630 nm indicating an exciton coupling, as also suggested by the red shifted shoulder at ~680 nm in the UV–vis spectra. UV–vis and CD spectra of **CSB/1/amine** assemblies including *n*-propylamine, 1,3-diaminopropane, putrescine or cadaverine do not show changes with respect to the spectra of **CSB/1** and are not reported. These results could suggest the requisite of a critical distance between amine functions and/or a critical number of amine functions to stabilize a specific configuration.

2.2. NMR experiments

Standard one-dimensional ^{1}H NMR experiments are a practical tool to monitor aggregation in solution [33]. Actually, aggregation affects the chemical shift and the linewidth of signals, possibly leading to their disappearance, as a consequence of changes in the mobility of molecules within the assembly. We compared the ^{1}H NMR spectra of the single components with those of the **CSB/1** mixtures both in the absence and in the presence of spermidine to verify self-assembling. In the spectra of the assemblies, signal broadening is observed (Fig. S2 in SI) both in the absence and in the presence of spermidine. Notably, due to line width enlargement, surfactant's signals are no more observable in the spectra of the assemblies, highlighting the formation of very large systems.

2.3. TEM imaging

Imaging of **CSB/1**, **CSB/1/spermidine** and **CSB/1/putrescine** assemblies was carried out to investigate their morphological features.

TEM experiments were performed on samples deposited both 30 min and 24 h after the preparation of the aqueous solutions.

Fig. 2 shows the images obtained from samples deposited after 30 min (*i.e.* under conditions similar to those used for CD spectroscopy). All images show very large architectures both in the presence and in the absence of polyamine. In the presence of spermidine (Fig. 2b) fibers can be observed (a higher magnification portion of the image is reported in SI as Fig. S3) that over time may evolve in longer fibers as observed in Fig. S4b of SI. Actually, all the samples show a higher extent of organization in the images taken at 24 h (Fig. S4 in the SI). It has not been possible to visualize chiral architectures.

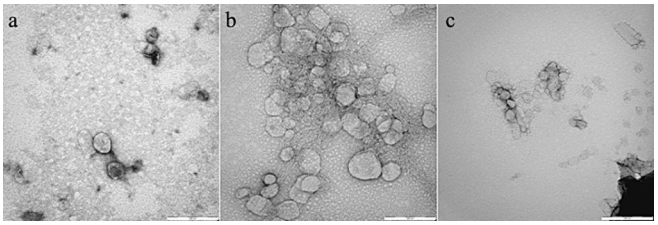

Fig. 2. TEM images of a) **CSB/1** assemblies; b) **CSB/1**/spermidine assemblies and c) **CSB/1**/putrescine assemblies obtained from samples deposited 30 min after the preparation of aqueous solutions. The scale size bar is 200 nm in all images.

2.4. Metadynamics simulations of dye/surfactant assemblies

To identify the entangled molecular interactions, we investigated the assemblies formed by a small number of molecules using enhanced sampling simulations within the framework of well-tempered [34] metadynamics [35]. These methods are extremely useful to capture sub-nanometer details and successfully predicted in the years the chiroptical features of chiral soft assemblies [36,37].

Herein we investigated how spermidine, norspermidine, spermine and putrescine modulate the chiral bias of **CSB** induced by the chiral surfactant through monitoring the rotation of the dihedral angle of central biphenyl moiety along with the two dihedral angles of azonaphthyl groups. The effect of the intermolecular interactions occurring in the actual assembly was considered by including a second molecule of **1** and **CSB** without applying any bias in order to follow how molecular rotations can be affected by a molecular chiral bias. Therefore, free-energy simulations were carried out on 2:2 dye/surfactant and 2:2:2 dye/surfactant/polyamine assemblies.

The free energy landscape associated to the rotation of the biphenyl and the two azonaphtyl groups of **CSB** was reconstructed (Fig. S5 in SI). The values of biphenyl and azonapthyl dihedral angles associated to free-energy minima of dye stereoisomers and the corresponding free energy values were identified (Table 1).

The absolute free energy minima of **CBS/1** aggregates were found at i) 180/±140/180 (*trans/trans/trans* - azonapthyl/biphenyl/azonapthyl) dihedral angle values, in the absence of polyamine, ii) 180/−50/180 in the presence of spermidine or spermine, iii) 180/+50/180 in the presence of norspermidine, and iv) 180/±50/180 in the presence of putrescine.

The *cis* conformers of azo-group dihedrals show a reduced stability compared to the *trans* ones, the free energy basins relative to *trans* and

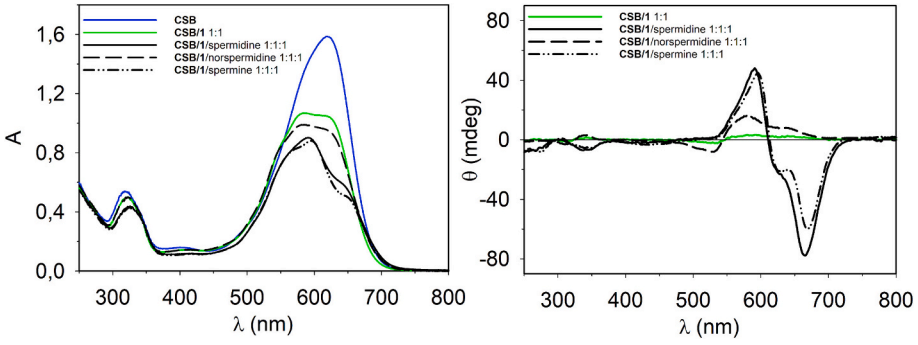

Fig. 1. UV–vis (left) and CD (right) spectra of an aqueous solution of 1:1:1 **CSB/1**/polyamine (spermidine, solid line; norspermidine, dash line; spermine dash-dot-dot line) run at 25 °C after incubation for 20 min at 25 °C. UV–vis spectrum of 20 μM **CSB** (blu trace) and the UV–vis and CD spectra of 1:1 **CSB/1** heteroaggregates (green trace). **1**, **CSB** and polyamine were 20 μM in all recorded spectra. (For interpretation of the references to color in this figure legend, the reader is referred to the web version of this article.)

Table 1
Values of biphenyl and azonaphtyl dihedral angles of **CSB** stereoisomers identifying a free-energy minimum and relative free-energy levels in the different assemblies. The absolute free-energy minima are marked in bold. Dihedrals and free-energy difference values reported are extrapolated from the 8 walker well-tempered metadynamics simulation. The associated error is estimated as 0.6 kcal/mol.

Azo_1	Biphenyl	Azo_2	ΔG^0 (kcal/mol)				
			CSB/1	CSB/1 Spermidine	CSB/1 Spermine	CSB/1 Norspermidine	CSB/1 Putrescine
180.0	+140.1	180.0	**0.0**	1.6	6.9	1.3	1.5
180.0	−140.1	180.0	0.7	3.5	1.2	3.2	1.6
180.0	+50.0	180.0	1.8	1.9	6.2	**0.0**	0.8
180.0	−50.0	180.0	1.6	**0.0**	**0.0**	5.1	**0.0**
0.0	+130.1	180.0	10.9	13.8	17.6	10.8	14.5
0.0	−130.1	180.0	12.4	14.5	11.3	13.9	12.7
180.0	+140.0	0.0	11.5	10.5	15.2	10.1	11.6
180.0	−140.0	0.0	12.0	13.9	11.7	13.6	12.6
180.0	+50.0	0.0	11.5	11.1	17.0	9.7	10.1
180.0	−50.0	0.0	12.8	9.7	11.8	11.9	9.9
0.0	+50.0	180.0	14.1	11.1	16.7	12.1	12.3
0.0	−50.0	180.0	12.2	16.6	9.7	13.9	11.4
−160.0	0.0	180.0	18.1	21.7	23.2	22.5	21.3
+160.0	0.0	180.0	18.9	21.8	22.8	22.3	21.3
−9.7	140.1	0.0	23.2	26.7	23.0	25.3	23.4
9.7	−140.1	0.0	21.5	24.1	26.2	24.7	22.2

cis isomers being separated in each landscape by an energy barrier reaching 50 kcal/mol (Fig. S5). The stereoisomers corresponding to the absolute free energy minima are stabilized compared to the stereoisomer of opposite configuration by ~2, 5 and 6 kcal/mol in the case of spermidine, norspermidine and spermine, respectively. This reveals a molecular deracemization resulting from a shift in the equilibrium of conformational enantiomers at the level of the biphenylic moiety. The extent of this shift is highest in the case of spermine.

Some significant structures of free-energy minima of **CSB/1** aggregates in the presence and in the absence of polyamine are reported in Fig. 3. In the absence of polyamine, **CSB** molecules are in a cross-shape arrangement that maximizes the distances between sulphonate groups whereas in the presence of spermidine, norspermidine and spermine the two molecules are aligned as the repulsive interactions of sulphonate groups are partially neutralized. In the presence of putrescine, the structures are characterized by a high variability ranging from almost cross shape (~77%) to aligned (~23%) arrangements as shown by two significant structures reported in Fig. 2e and Fig. 2f, suggestive of a very modest neutralization of sulphonate groups. These results clearly demonstrate that the presence of the polyamines and their nature strongly influence the organization of **CSB/1** aggregates, their energy patterns and the chiral bias.

2.5. Simulated CD spectra

The accuracy of the predictions on the aggregate organization was assessed through the calculation of electronic CD spectra at the ZINDO level, with a good compromise between computational demand and reliability in predicting the ECD spectra of chiral frameworks [38,39]. ECD spectra were calculated on free-energy minima. It is known that both semi-empirical and TD-DFT simulation methods can overestimate excitation energies resulting in a blue shift of the calculated spectra, thus requiring the typical inclusion of a shift term in spectral simulations [38,40].

The calculated spectra, that include a shift term, are reported in Fig. 4. An intense negative exciton couplet is predicted when two naphtyls are stacked with an anticlockwise rotational shift and the intensity of the band is predicted to increase when the extent of π-stacking is higher. The most intense couplets are predicted for assemblies including spermidine and spermine, both centered at ~640 nm. A modest positive band is predicted for the assemblies including norspermidine. No CD bands are predicted in the absence of polyamine and in the case of the assembly including putrescine. The correspondence between experimental and theoretical spectra is good if we consider that some differences might arise due to thermal contributions and solvent effects.

2.6. Intermolecular interactions

Given the good convergence between experimental and theoretical results, details on the organization of the various assemblies can be safely extrapolated by analyzing the structures of the free energy minima and measuring the averaged distances between the centroids of functional groups of surfactant and dye molecules.

In the absence of polyamine **CSB** molecules are quite far apart in their cross topology (the average distance between the center of mass of 1–1′ carbon atoms of biphenyl aromatic rings being 13 Å), with molecules of **1** in between them spreading out their alkyl chains along dye molecules.

In the presence of spermidine, norspermidine and spermine, in the aligned arrangement of **CSB** molecules two naphthyls of different dye molecules give π-stacking with an average distance between their centroids of 4.2 Å. At the other end of the assemblies, the planes of the other two naphthyls are almost perpendicular to each other. However, some crucial differences arise from the different molecular structure of the polyamines, that control their consequent arrangement in the assemblies and the overall arrangement of the assemblies.

Both molecules of spermidine are positioned on the side of stacked naphtyls, their main axes being perpendicular to the planes of naphtyls, and both engage nitrogen atoms on 1 and 3 position (*i.e* separated by a three-methylene residue) in 'clip' interactions, each one of which grips two sulphonate groups exposed on parallel naphtyls in *gauche* like orientation (Fig. 5a). At the other end of the assembly repulsive interactions keep far apart the sulphonate groups. Both clipping of naphtyls on one side of the assembly and electrostatic repulsion on the other side generate a rotation of the plane of one stacked naphtyl with respect to the plane of the other naphthyl to yield an anti-clockwise helix (stabilized with respect to the enantiomeric one by interactions with the chiral surfactant, at 5.1 Å from the stacked naphtyls), and attribute a helical shape to the whole assembly.

Differently, the molecules of spermine and norspermidine are located at both ends of the assemblies and the stacked naphtyls are antiparallel with amine groups in *anti* like orientation. This topology involves only eclipsing of functional groups of opposite charge. Furthermore, the main axes of both polyamines are kind of parallel to the planes of stacked naphtyls and each amine group interacts with

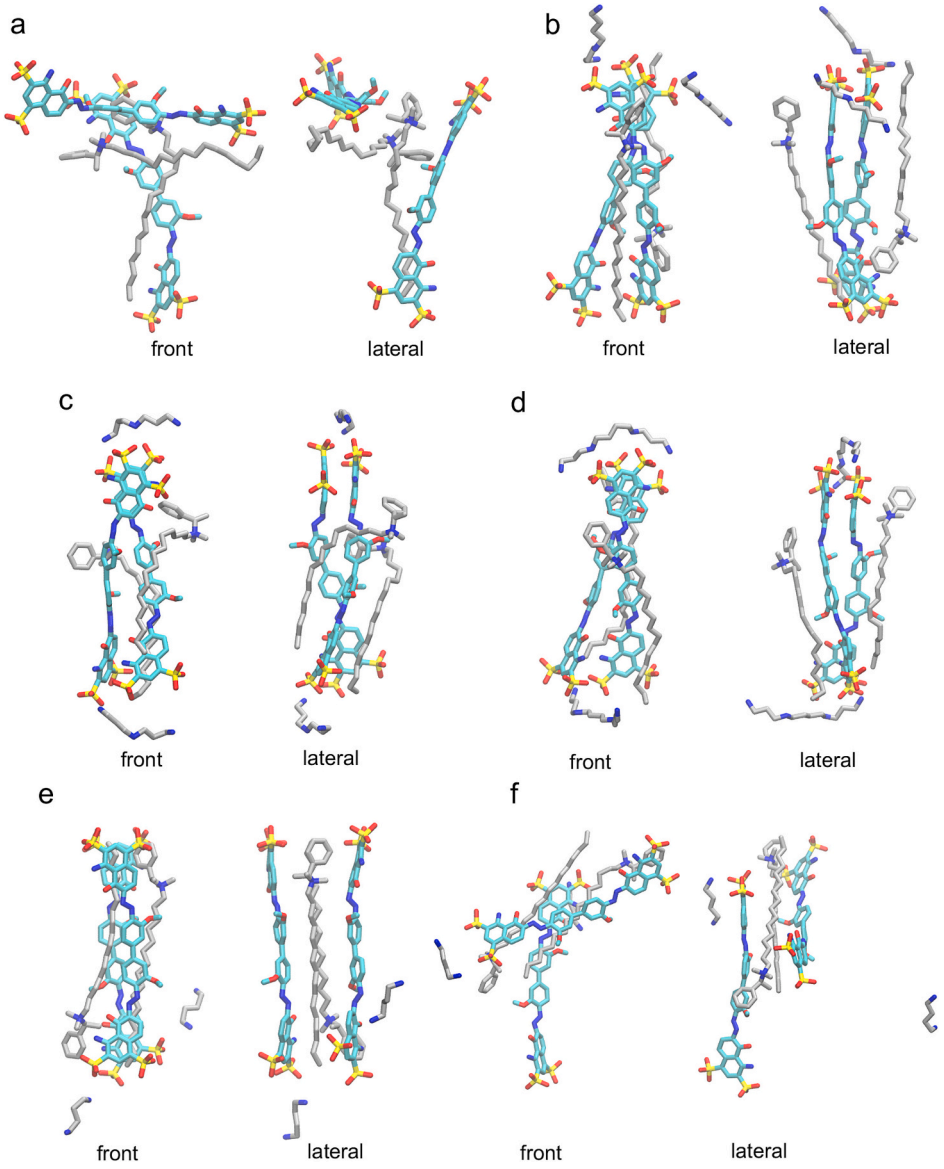

Fig. 3. Significative structures of free-energy minima of **CSB**/**1** assemblies in a) the absence of polyamines and in the presence of b) spermidine, c) norspermidine, d) spermine, e) putrescine (aligned arrangement), f) putrescine (cross shape arrangement). The molecules are represented in sticks and colored according to their atom types (red-oxygen, blue-nitrogen, yellow-sulfur atoms, cyan-carbon atoms of **CSB** and silver-carbon atoms of **1** and polyamines). (For interpretation of the references to color in this figure legend, the reader is referred to the web version of this article.)

sulphonates exposed on both stacked naphtyls. Spermine mainly engages each of its two pairs of amine groups, located at positions 1 and 3, and 7 and 10 (N atoms of each pair separated by a three-methylene residue), with different pairs of sulfonates on parallel naphthyl rings. Norspermidine engages each amine group in 3 and 6 positions with three sulphonate groups, and the central amine group with four. However, while in the presence of spermine all sulphonate groups are at a distance $<$4.5 Å from at least one of the amino groups, in the case of norspermidine one of the sulphonate groups of the dye is at a distance $\geq$7.5 Å from all the amino groups. In the case of spermine it is possible to appreciate a slight rotational shift of naphtyls, probably due to the efficient electrostatic interactions between amino groups and sulphonate groups of stacked naphthyls. The other molecule of norspermidine or spermine interacts with sulphonates groups at the other end of the assembly, thus decreasing electrostatic repulsion and yielding a more compact shape of the assembly with respect to that including spermidine.

In the presence of putrescine, the aggregate organization markedly differs from those described above. The two **CSB** molecules are well-separated, with molecules of **1** positioned between them in a head to tail arrangement. This stands in contrast to the other assemblies where they are tangled up with **CSB** molecules. Putrescine molecules do not interact closely with sulfonate groups, however partial neutralization occurs allowing **CSB** molecules to occasionally adopt an aligned arrangement, differently from what found in the absence of amine.

This analysis has identified some key interactions that might control the handedness of the assembly induced by the chiral surfactant. On the one hand spermidine engages two out of its three amine functions in clipping coulombic interactions with sulphonate groups, spermine exploits its four amine functions in defined pairs to interact with different pairs of sulphonate groups and norspermidine engages all its three amine functions. Interestingly in all the polyamines the amine groups performing as a pair are separated by three methylenes. On the other hand, putrescine, where amine functions are separated by a four-methylene chain, interacts very loosely with sulphonate groups. These observations could suggest that the presence of two amine functions

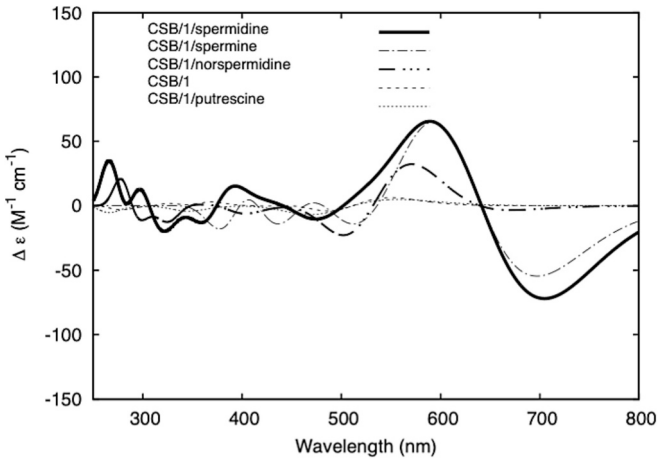

Fig. 4Data in strikethrough have been retained. Please check if this is appropriate. CD spectra calculated on the free-energy minima identifying the azonaphtyl groups in the *trans* and *cis* conformations.

linked by a three-methylene chain might be the critical feature enabling concurrent interaction with two molecules of dye. However, **CSB/1** assemblies are CD silent in the presence of 1,3-diaminopropane. Therefore, the synergy of two amine functions at a given intramolecular distance is important but not sufficient and the other amine groups contribute to the specificity of the interaction and to the topology of the assembly. Additional coulombic interactions between amine and sulphonate functions can be found in the structures of the energy minima. For example, the amine function on position 7 of one of the molecules of spermidine reinforces the clip action of the pair of amine groups by interacting with one of the clipped sulphonates. In the case of spermine, the amine function on 3 position interacts with two sulphonates on different naphtyls at a shorter distance (as discussed above) and with a third one at a larger distance. Other interactions involve amine groups in 7 and 10 positions of spermine and the amine groups of norspermidine, as evidenced in Fig. 5.

2.7. *Molecular electrostatic potentials (MEP) of polyamines*

The molecular structure of the investigated polyamine, and hence the number of amine functions and their intramolecular spacing influences their conformational flexibility and their electrostatic potential

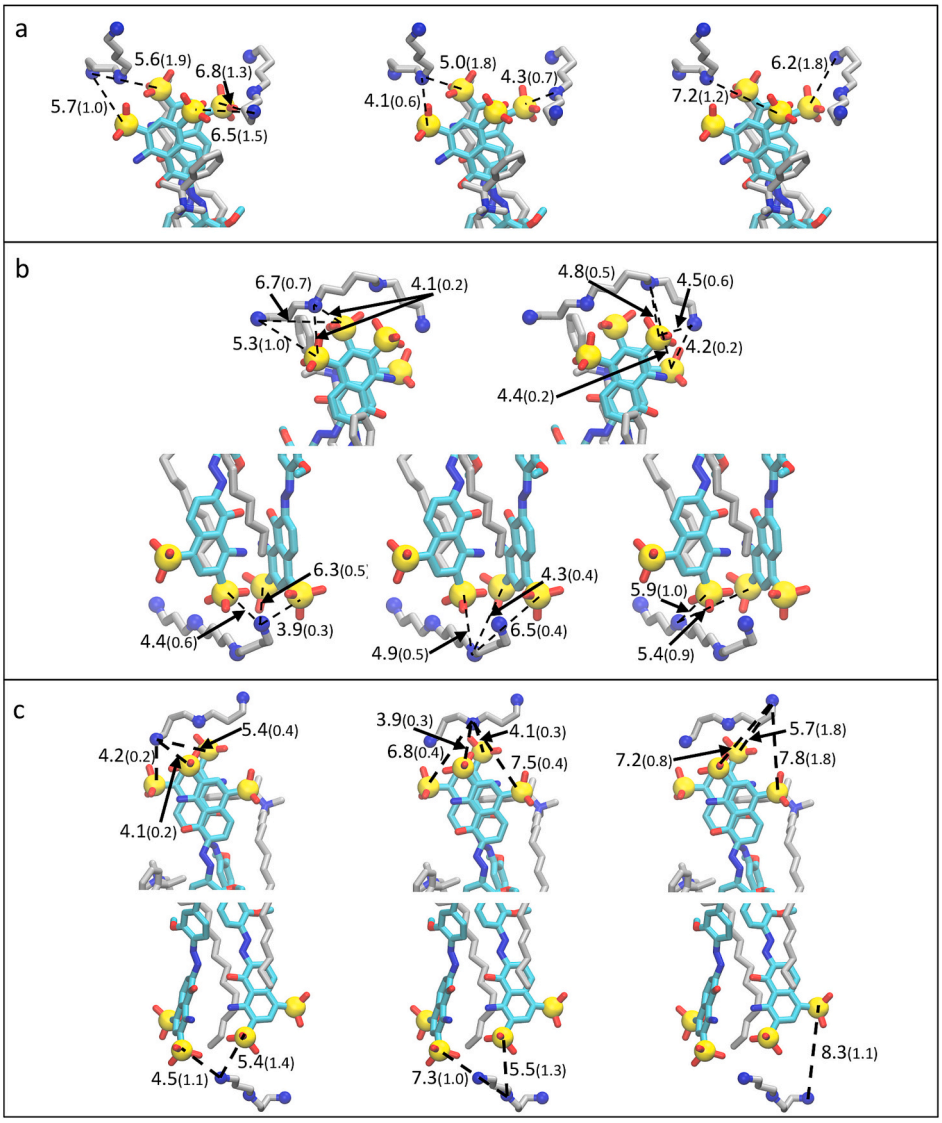

Fig. 5. Average orientation of polyamines in the free-energy minima of **CSB/1** heteroaggregates: a) spermidine, b) spermine, c) norspermidine. The average distance (in Å) between the nitrogen atoms of polyamines and the sulfur atoms of **CSB**, with the relative standard deviation (in parentheses) are reported.

thus ultimately controlling their interaction with the **CSB/1** assemblies. To elucidate these effects, we calculated the MEPs of all the polyamines reported in Chart 1, as well as that of 1,3-diaminopropane. Calculations were performed for the all-trans conformations and, in the case of spermidine, spermine, and norspermidine, also for the conformations observed within the free-energy minima where they interact with stacked naphthyl groups. Fig. 6 reports the comparison of the electrostatic potentials calculated in the case of the trans conformations: the highest electrostatic potentials are observed, in decreasing order, for spermine, norspermidine and spermidine, whereas significantly lower values are observed for 1,3-diaminopropane, putrescine and cadaverine. It is clear from the maps of electrostatic potential that the 1–3 spacer is a key element for an effective interaction only in the presence of a third amino group, at least. This finding could rationalize the results obtained in the UV–vis and CD experiments and in the metadynamics simulations. Actually, as mentioned above, UV–vis and CD spectra of **CSB/1**/amine assemblies including 1,3-diaminopropane, putrescine or cadaverine are identical to those of **CSB/1** and this is evidently due to the fact that, because of their low electrostatic potential, these amines do not interact efficiently with the **CSB/1** assembly. Further, the structures of free energy minima obtained by metadynamics simulations confirmed that putrescine interacts very loosely with the **CSB/1** assembly affecting its arrangement to a low extent.

Fig. 7 reports the electrostatic potentials of spermidine, spermine and norspermidine in the conformations found within the structures of the free energy minima of the assemblies. The comparison shows that the amino group of spermidine in position 7 features the lowest electrostatic potential, thus justifying the engagement of two molecules to efficiently neutralize the sulphonate groups of the dye.

3. Conclusions

The outcome of a CD investigation showed that polyamines can differently shape the chiroptical properties of assemblies formed by **CSB** and a chiral enantiopure cationic surfactant; hence we performed a theoretical study focusing on small aggregates to determine the minimal structural units required to give a measurable CD response. The **CSB/surfactant** assembly is organized in a cross-shape pattern that trasforms into an aligned pattern in the presence of specific polyamines. Both patterns can potentially grow taking on a chiral shape. The detection of a supramolecular architecture chirality depends on many parameters, such as intermolecular distances and π-stacking geometry that produce an exciton coupling, clearly detectable by CD. In assemblies that do not exhibit a supramolecular chiral shape still CD spectroscopy can detect chirality, this time in the form of an enantiomeric excess at molecular level yielded by the deracemization of one or more chiral conformations of the dye.

The CD spectra of **CSB/1** assemblies including spermidine and spermine might be diagnostic of the deracemization of a supramolecular helix formed by the rotational shift of stacked naphtyls. In the case of spermidine the formation of the helix can be ascribed to clipping of sulphonate groups by the molecules of polyamine on one end of the assembly and to Coulombic repulsion and conformational freedom on the other end, whereas in the case of spermine it can be ascribed to the efficient neutralization of sulphonate groups of stacked naphtyls by a single molecule of polyamine. In both cases the observed handedness of the helix is induced by the chiral surfactant through various intermolecular interactions.

In the absence of polyamine and in the presence of norspermidine the pattern of the CD spectrum is different and could indicate exclusively deracemization of the biphenyl moiety, as also indicated by calculations, and/or of other chiral conformations of the dye.

This study suggests that non chiral metabolites featuring key functional groups can be crucial in the transcription of the genetically codified handedness of natural systems. While chiral templates are fundamental, their functional expression may depend on the presence of specific non-chiral cofactors. Therefore, in our model we would not observe any deracemization, either at the molecular or at the supramolecular level, if the surfactant (our template) were not chiral; however specific polyamines shape and enhance the extent of deracemization.

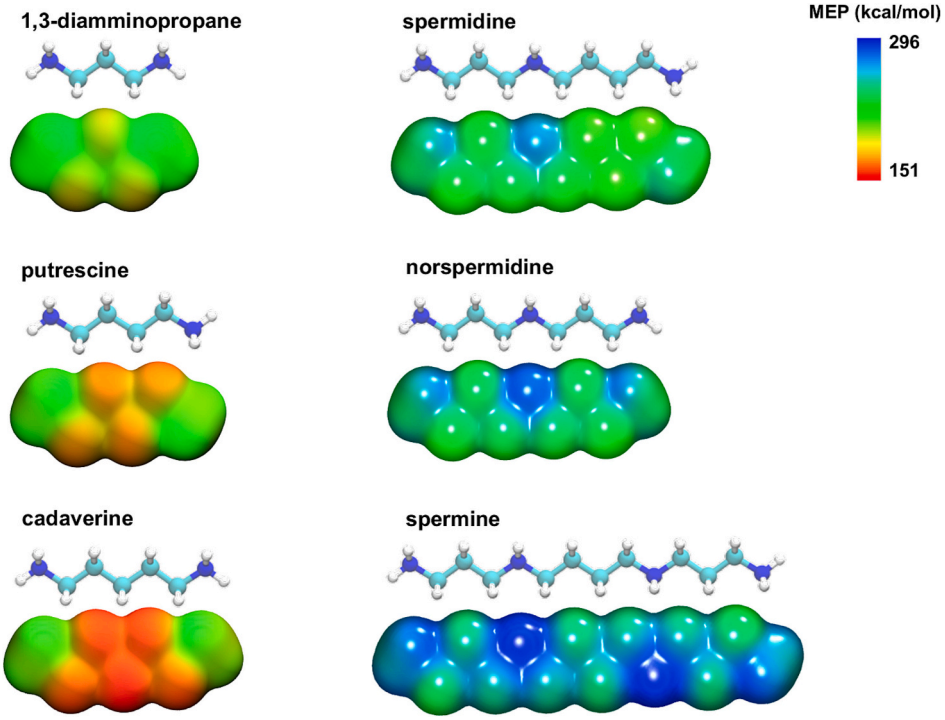

Fig. 6. MP2/6–31 G(d,p) MEP (0.001 isodensity surface) of the investigated polyamines in all trans conformation. Values in the color bar are in kcal/mol.

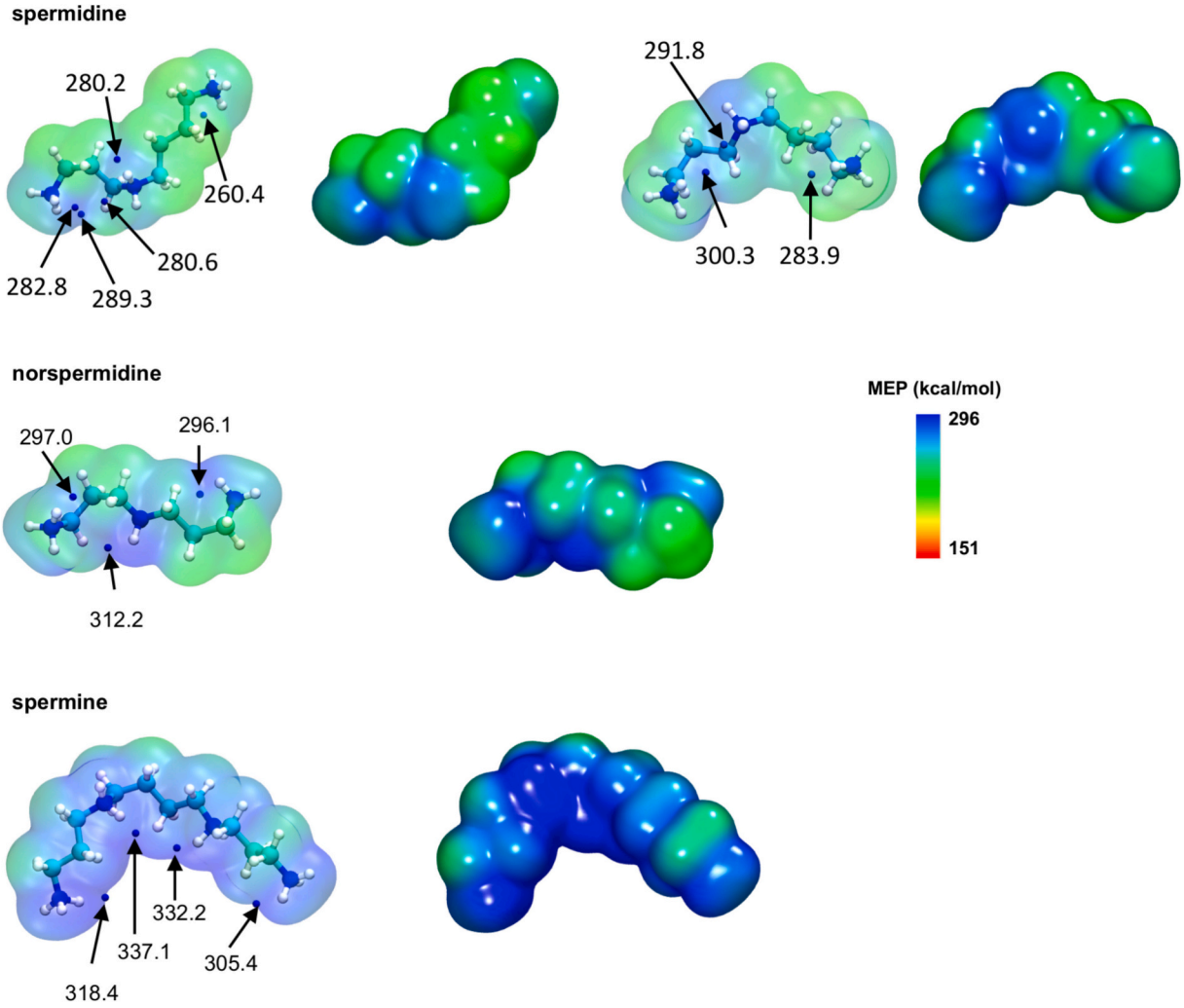

Fig. 7. MP2/6–31 G(d,p) MEP (0.001 isodensity surface) of spermidine, norspermidine and spermine calculated on the representative conformation of polyamines on the free energy minima obtained by metadynamics simulations. Values in the color bar and the reported calculated maximum points of the electrostatic potential (*Vs*,max) are in kcal/mol.

4. Materials and methods

4.1. Materials

Chicago Sky Blue (**CSB**), 1,3-propandiamine, 1,5-pentandiamine (cadaverine), bis-(3-aminopropyl)amine (norspermidine), 1,4-butandiamine (putrescine), N-(3-aminopropyl)butan-1,4-diamine (spermidine) and *N*,*N*′-bis(3-aminopropyl)butan-1,4-diamine (spermine) were purchased from Sigma Aldrich.

Chiral cationic surfactant (*S*)-*N*,*N*-dimethyl-N-(1-phenylethyl)-esadecan-1-ammonium bromide (**1**) was prepared following a procedure reported in the literature.

Milliq water was used for sample preparations. D_2O was purchased from Sigma-Aldrich.

4.2. Sample preparation

For sample preparation, 1.0 mM stock solutions of **CSB**, **1** and poliamines in Milliq water were prepared. The protocol of addition was the following: 60 μL of 1.0 mM **1** solution were diluted with MilliQ water to 2880 μL, then 60 μL of 1.0 mM **CSB** were added and the resulting solution thoroughly stirred, finally 60 μL of 1.0 mM polyamine were added. For **CSB**/**1** aggregates in the absence of poliamine, after addition of the dye, 60 μL of MilliQ water were added. The volumes were chosen to have 3.0 mL of the final solution with [**CSB**] = [**1**] = [polyamine] = 20 μM. After mixing the components, samples were left to incubate for 20 min at 25 °C or heated to 50 °C for 30 min before being analyzed.

4.3. UV–vis and CD experiments

Absorption spectra were recorded on a Cary 300 UV–vis double beam spectrophotometer whereas CD spectra were recorded on a Jasco spectropolarimeter J-715, both equipped with a Peltier device for temperature control.

CD spectra are the average of 16 scans obtained with an instrument scanning speed of 100 nm/min, response time of 1 s, and resolution of 1 nm.

CD and UV spectra were recorded at 25 °C in the 800–250 nm spectral range, using 1.0 cm path length quartz cuvette. Because previous investigations showed that the CD spectra of dye/surfactant assemblies recorded shortly after preparation differ from those recorded after equilibration of samples at 50 °C [41], samples were analyzed 20 min (at 25 °C) after preparation and after heating for 30 min at 50 °C (see SI).

4.4. NMR measurements

NMR spectra were recorded at 27 °C on a Bruker AVANCE 600

spectrometer operating at a proton frequency of 600.13 MHz.

Samples were prepared in deuterated water and then treated before analysis as described above.

Presaturation during the relaxation delay was used to suppress the water signal.

4.5. Transmission electron microscopy (TEM)

The morphology of the heteroaggregates was analyzed using transmission electron microscopy, employing the negative staining technique, which allows the structure to be observed in bright field against the background of heavy metal staining.

The samples (10 μL) were dropped onto a copper grid coated with carbon-coated Formvar, 30 min and 24 h after preparation respectively, and left to adsorb for 60 s.

The grid was first immersed in a drop of 2% (*w/v*) aqueous uranyl acetate solution for 150 s, then in a drop of distilled water and finally in another drop of uranyl acetate for 60 s. After gently removing the excess solution, the samples were rapidly air-dried. The entire procedure was carried out at room temperature, and the resulting grid was then imaged using a JEOL 1200 EX II electron microscope. The micrographs were captured using an Olympus SIS VELETA CCD camera equipped with Olympus software.

4.6. Simulation details

The assemblies investigated were composed by two molecules of **CSB**, two molecules of the (*S*)-*N,N*-dimethyl-*N*-(1-fenyl-etyl)esadecane-1-ammonium ion (**1**) and two molecules of each of one of the investigated polyamines, namely spermidine, spermine, norspermidine and putrescine. To reproduce the experimental conditions at neutral pH, amine groups were modeled in their protonated state. All the systems were solvated adding 5239 water molecules and the net excess charge was neutralized adding chloride or sodium ions where necessary (*i.e.* no counterions in the case of spermidine and norspermidine, two chloride ions in the case of spermine and two sodium ions in the case of putrescine). The dye/surfactant heteroaggregate in the absence of polyamine was also considered for comparison, six sodium ions were added to guarantee charge neutrality.

All the structures were initially equilibrated through 10 ns of MD at 300 K, followed by 10 ns of steered molecular dynamics (SMD) along the three torsions belonging to the biphenyl and the two naphtyl groups. The eight diastereoisomers, (*trans-trans-trans*, *trans-cis-trans*, *trans-trans-cis*, *trans-cis-cis*, *cis-trans-trans*, *cis-cis-trans*, *cis-trans-cis*, *cis-cis-cis*) were then modeled. The C_2 symmetry breaking owing to the interactions of **CSB** with the chiral surfactant **1** originates the diastereoisomers *cis-trans-trans/trans-trans-cis and cis-cis-trans/trans-cis-cis*.

Well-tempered [34] metadynamics [35] simulations were run using as collective variables the torsion of the biphenyl and of the two naphtyl groups in one of **CSB** molecules. Multiple walkers [42] methodology was used to accelerate the free energy convergence. Eight walkers were considered in order to represent all the diastereoisomers in the other **CSB** molecule where no metadynamics bias was applied. Gaussians with a height of 0.6 kcal/mol were deposited at 1 ps time interval, with a bias factor equal to 10. Periodic boundary conditions were applied throughout the simulations to minimize finite-size effects.

NVT ensemble with a temperature of 300 K were enforced using a Langevin thermostat, as implemented in the GROMACS molecular dynamics code - version 2016.3 [43] Electrostatic interactions were calculated using the Particle Mesh Ewald method [44]. The time-step was set to 2 fs. The LINCS algorithm [45] was applied to fix all bond lengths. Good convergence of the free-energy surfaces was obtained in the Well Tempered-Metadynamics runs, and recrossing multiple times between the *cis* and *trans* states (Fig. S3 in SI).

The potential developed by Böckmann et al. for naphtyl torsions [41] was used to treat the naphtyl units, the potential of Karpfen et al. [46] was used to treat the biphenyl units, the AMBER99SB potential was used to treat the other part of the molecules and the counterions. TIP3P potential [47] was used for water molecules. The ESP charges of the surfactant molecule were calculated using Gaussian16 [48] on the optimized structures at the Hartree-Fock (HF) level within the 6–31G(d) basis sets [28].

4.7. Calculations of electronic CD and UV spectra

The intrinsic rotatory strengths were calculated for the conformations belonging to the main free-energy minima of the **CSB/1**/polyamines heteroaggregate simulations.

ECD spectra calculations were run using Gaussian 16 package. Fifty singlet excited states of the **CSB/1**/polyamine and C**SB/1** were calculated using the ZINDO semiempirical parametrization [49–51]. The rotatory strengths are reported in the usual c.g.s. units of 10^{-40} esu.cm. erg/G.

The calculations of the ECD spectra at a given wavelength, λ, were carried out assuming Gaussian bands with 1400 cm^{-1} full width at half-height (from 200 nm to 800 nm) for all transitions centered in a given excitation wavelength. A factor of 2.278 was applied during the conversion of rotatory strengths and Δε values, as reported previously [51,52]. The CD intensities of the conformers belonging to the main free-energy mimina with the azide groups in *trans* and *cis* conformation were averaged according to the weight of each free-energy minimum through eq.1, where ϕ_1, ϕ_2, ϕ_3 are the biphenyl and the two naphtyl group torsions, β is the inverse of the kT term, k being the Boltzmann constant.

$$< CD_\lambda >= \frac{\sum CD_\lambda e^{-\beta F(\phi_1,\phi_2,\phi_3)}}{\sum e^{-\beta F(\phi_1,\phi_2,\phi_3)}} \quad (1)$$

4.8. Calculation of molecular electrostatic potentials (MEP)

The molecular electrostatic potential (MEP) on the 0.001 ea_0^{-3} electron density isosurface of polyamines were calculated at the MP2/6–31 G(d,p) level of theory by using the wavefunction generated by Gaussian 16 package and analyzed with Multiwfn program [53].

Author contribution

G.M. conceived the work, supervised this research and wrote the first draft of the paper. A.P. planned and carried out the theoretical calculations. S.B. was responsible for the detailed analysis of molecular interactions from calculation output. B.S. and F.C. planned and carried out the experimental Uv and CD experiments. S.P. carried out the preliminary CD experiments. M.M. was responsible for the NMR investigation. All authors contributed to discussion of results and to revision and editing of the manuscript.

CRediT authorship contribution statement

Francesca Ceccacci: Writing – review & editing, Methodology, Investigation, Data curation. **Beatrice Simonis:** Writing – review & editing, Methodology, Investigation, Data curation. **Serena Ponte:** Investigation. **Marco Mazzonna:** Writing – review & editing, Methodology, Investigation. **Adriana Pietropaolo:** Writing – review & editing, Investigation, Formal analysis, Conceptualization. **Stefano Borocci:** Writing – review & editing, Methodology, Formal analysis, Data curation. **Giovanna Mancini:** Writing – review & editing, Writing – original draft, Supervision, Project administration, Conceptualization.

Declaration of competing interest

The authors declare that they have no known competing financial interests or personal relationships that could have appeared to influence the work reported in this paper.

Acknowledgments

We thank Dr. Anna Rita Taddei who conducted the TEM experiments at the Centro Grandi Attrezzature (CGA) of Tuscia University.

Appendix A. Supplementary data

Supplementary data to this article can be found online at https://doi.org/10.1016/j.jcis.2026.140629.

Data availability

No data was used for the research described in the article.

References

[1] L. Addadi, S. Weiner, Crystals, asymmetry and life, Nature 411 (2001) 753–755.
[2] C.A. Orme, A. Noy, A. Wierzbicki, M.T. McBride, M. Grantham, H.H. Teng, P. M. Dove, J.J. DeYoreo, Formation of chiral morphologies through selective binding of amino acids to calcite surface steps, Nature 411 (2001) 775–779.
[3] A. Levy-Lior, S. Weiner, L. Addadi, Achiral calcium-oxalate crystals with chiral morphology from the leaves of some solanacea plants, Helv. Chim. Acta 86 (2003) 4007–4017.
[4] R. Kuroda, B. Endo, A. Masanori, M. Shimuzu, Chiral blastomere arrangement dictates zygotic left–right asymmetry pathway in snails, Nature 462 (2009) 790–795.
[5] H. Lu, A. Schäfer, H. Lutz, S.J. Roeters, I. Lieberwirth, R. Muñoz-Espí, M.A. Hood, M. Bonn, T. Weidner, Peptide-controlled assembly of macroscopic calcium oxalate nanosheets, J. Phys. Chem. Lett. 10 (2019) 2170–2174.
[6] Y. Ma, L. Shi, H. Yue, X. Gao, Recognition at chiral interfaces: from molecules to cells, Colloids Surf. B Biointerfaces 195 (2020) 111268.
[7] W. Jiang, M.S. Pacella, D. Athanasiadou, V. Nelea, H. Vali, R.M. Hazen, J.J. Gray, M.D. McKee, Chiral acidic amino acids induce chiral hierarchical structure in calcium carbonate, Nat. Commun. 8 (2017) 15066.
[8] U. Hananel, A. Ben-Moshe, D. Tal, G. Markovich, Enantiomeric control of intrinsically chiral nanocrystals, Adv. Mater. 32 (2020), 3e1905594-1905599.
[9] W. Jiang, M.S. Pacella, H. Vali, J.J. Gray, M.D. McKee, Chiral switching in biomineral suprastructures induced by homochiral l-amino acid, Sci. Adv. 4 (2018) eaas9819.
[10] E.A. Perets, D. Konstantinovsky, L. Fu, J. Chen, H.-F. Wang, S. Hammes-Schiffer, E. C.Y. Yan, Mirror-image antiparallel β-sheets organize water molecules into superstructures of opposite chirality, Proc. Natl. Acad. Sci. U. S. A. 117 (2020) 32902–32909.
[11] H. Kim, S.W. Im, R.M. Kim, N.H. Cho, H.-E. Lee, H.-Y. Ahn, K.T. Nam, Chirality control of inorganic materials and metals by peptides or amino acids, Mater. Adv. 1 (2020) 512–524.
[12] S.M. Morrow, A.J. Bissette, S.P. Fletcher, Transmission of chirality through space and across length scales, Nat. Nanotechnol. 12 (2017) 410–419.
[13] W. Jiang, X. Yi, M.D. McKee, Chiral biomineralized structures and their biomimetic synthesis, Mater. Horiz. 6 (2019) 1974–1990.
[14] M. Liu, L. Zhang, T. Wang, Supramolecular chirality in self-assembled systems, Chem. Rev. 115 (2015) 7304–7397.
[15] I. Danila, F. Riobe, F. Piron, J. Puigmarti-Luis, J.D. Wallis, M. Linares, H. Agren, D. Beljonne, D.B. Amabilino, N. Avarvari, Hierarchical chiral expression from the nano- to mesoscale in synthetic supramolecular helical fibers of a nonamphiphilic C_3-symmetrical π-functional molecule, J. Am. Chem. Soc. 133 (2011) 8344–8353.
[16] F.J.M. Hoeben, P. Jonkheijm, E.W. Meijer, A.P.H.J. Schenning, About supramolecular assemblies of π-conjugated systems, Chem. Rev. 105 (2005) 1491–1546.
[17] N. Ousaka, Y. Takeyama, H. Iida, E. Yashima, Chiral information harvesting in dendritic metallopeptides, Nat. Chem. 3 (2011) 856–861.
[18] F. Wang, H. Qiu, C. Feng, Wrapping chiral nanoribbons into coiled and condensed microstructures in supramolecular hydrogels, Adv. Funct. Mater. 30 (2020) 2002936.
[19] S. Zheng, G. Liu, Hierarchical self-assembly promoted circularly polarized luminescence enhancement and handedness inversion of metal–organic helicate, CCS Chem. 6 (2024) 2198–2209.
[20] G. Liu, M.G. Humphrey, C. Zhang, Y. Zhao, Self-assembled stereomutation with supramolecular chirality inversion, Chem. Soc. Rev. 52 (2023) 4443–4487.
[21] K. Fu, D.-H. Qu, G. Liu, Reversible circularly polarized luminescence inversion and emission color switching in photo-modulated supramolecular polymer for multi-modal information encryption, J. Am. Chem. Soc. 146 (2024) 33832–33844.
[22] K. Fu, Y. Zhao, G. Liu, Pathway-directed recyclable chirality inversion of coordinated supramolecular polymers, Nat. Commun. 15 (2024) 9571.
[23] Y. Sang, M. Liu, Hierarchical self-assembly into chiral nanostructures, Chem. Sci. 13 (2022) 633–656.
[24] H. Moorthy, L. Priya Datta, T. Govindaraju, Molecular architectonics-guided design of biomaterials, Chem. Asian J. 16 (2021) 423–442.
[25] F. Ceccacci, G. Mancini, A. Sferrazza, C. Villani, pH variation as the switch for chiral recognition in a biomembrane model, J. Am. Chem. Soc. 127 (2005) 13762–13763.
[26] H. Nakagawa, Y. Kobori, M. Yoshida, K. Yamada, Chiral recognition by single bilayered phosphatidylcholine vesicles using [5]thiaheterohelicene as a probe, Chem. Commun. (2001) 2692–2693.
[27] C. Bombelli, C. Bernardini, G. Elemento, G. Mancini, A. Sorrenti, C. Villani, Concentration as the switch for chiral recognition in biomembrane models, J. Am. Chem. Soc. 130 (2008) 2732–2733.
[28] F. Marinelli, A. Sorrenti, V. Corvaglia, V. Leone, G. Mancini, Molecular description of the propagation of chirality from molecules to complex systems: different mechanisms controlled by hydrophobic interactions, Chem. A Eur. J. 18 (2012) 14680–14688.
[29] F. Ceccacci, L. Giansanti, G. Mancini, A. Mauceri, A. Scipioni, C. Sperduto, Transcription of chirality from molecules to complex systems: the role of hydrophobic interactions, Supramol. Chem. 25 (2013) 741–747.
[30] F. Ceccacci, A. Scipioni, B. Altieri, L. Giansanti, G. Mancini, Achiral dye/surfactant heteroaggregates for chiral sensing of phosphocholines, Chirality 28 (2016) 22–28.
[31] R.T. Buwalda, J.B.F.N. Engberts, Aggregation of dicationic surfactants with methyl orange in aqueous solution, Langmuir 17 (2001) 1054–1059.
[32] A.R. Tehrani Bagha, H. Bahrami, B. Movassagh, M. Arami, F.M. Menger, Interactions of gemini cationic surfactants with anionic azo dyes and their inhibited effects on dyeability of cotton fabric, Dyes Pigm. 72 (2007) 331–338.
[33] J.R. Murugesan, F. Shahout, M. Dlim, M.M. Langella, E. Cuadra-Foy, P. Forgione, S. R. LaPlante, Revealing dye and dye-drug aggregation into nano-entities using NMR, Dyes Pigments 153 (2018) 300–306.
[34] A. Barducci, G. Bussi, M. Parrinello, Well-tempered metadynamics: a smoothly-converging and tunable free-energy method, Phys. Rev. Lett. 100 (2008) 020603.
[35] A. Laio, M. Parrinello, Escaping free-energy minima, Proc. Natl. Acad. Sci. U. S. A. 99 (2002) 12562–12566.
[36] A. Pietropaolo, D. Branduardi, M. Bonomi, M. Parrinello, A chirality-based metrics for free-energy calculations in biomolecular systems, J. Comput. Chem. 32 (2011) 2627–2637.
[37] M. Fortino, C. Cozza, M. Bonomi, A. Pietropaolo, Multi-replica biased sampling for photoswitchable π-conjugated polymers, J. Chem. Phys. 154 (2021) 174108.
[38] R. Bauernschmitt, R. Ahlrichs, Treatment of electronic excitations within the adiabatic approximation of time dependent density functional theory, Chem. Phys. Lett. 256 (1996) 454–464.
[39] R. Andreani, C. Bombelli, S. Borocci, J. Lah, G. Mancini, P. Mencarelli, G. Vesnaver, C. Villani, New biphenylic derivatives: synthesis, characterisation and enantiodiscrimination in chiral aggregates, Tetrahedron Asymmetry 15 (2004) 987–994.
[40] F. Furche, R. Ahlrichs, C. Wachsmann, E. Weber, A. Sobanski, F. Voegtle, S. Grimme, Circular dichroism of helicenes investigated by time-dependent density functional theory, J. Am. Chem. Soc. 122 (2000) 1717–1724.
[41] M. Böckmann, C. Peter, L.D. Site, N.L. Doltsinis, K. Kremer, D. Marx, Atomistic force field for azobenzene compounds adapted for QM/MM simulations with applications to liquids and liquid crystals, J. Chem. Theory Comput. 3 (2007) 1789–1802.
[42] P. Raiteri, A. Laio, F.L. Gervasio, C. Micheletti, M. Parrinello, Efficient reconstruction of complex free energy landscapes by multiple walkers metadynamics, J. Phys. Chem. B 110 (2006) 3533–3539.
[43] B. Hess, C. Kutzner, D. van der Spoel, E. Lindahl, GROMACS 4: algorithms for highly efficient, load-balanced, and scalable molecular simulation, J. Chem. Theory Comput. 4 (2008) 435–437.
[44] U. Essmann, L. Perera, M.L. Berkowitz, T. Darden, H. Lee, L.G. Pedersen, A smooth particle mesh Ewald method, J. Chem. Phys. 103 (1995) 8577–8593.
[45] B. Hess, P-LINCS: a parallel linear constraint solver for molecular simulation, J. Chem. Theory Comput. 4 (2008) 116–122.
[46] A. Karpfen, C.H. Choi, M. Kertesz, Single-bond torsional potentials in conjugated systems: a comparison of *abInitio* and density functional results, J. Phys. Chem. 101 (1997) 7426–7433.
[47] W.L. Jorgensen, J. Chandrasekhar, J.D. Madura, R.W. Impey, M.L. Klein, Comparison of simple potential functions for simulating liquid water, J. Chem. Phys. 79 (1983) 926–935.
[48] M.J. Frisch, et al., Gaussian 16, Revision B.01, Gaussian, Inc., Wallingford CT, 2016.
[49] J.E. Ridley, M.C. Zerner, An intermediate neglect of differential overlap technique for spectroscopy: pyrrole and the azines, Theor. Chim. Acta 32 (1973) 111–134.
[50] J.E. Ridley, M.C. Zerner, The calculated spectra of the azanaphthalenes, J. Mol. Spectrosc. 50 (1974) 457–473.
[51] N. Sreerama, R.W. Woody, Computation and analysis of protein circular dichroism spectra, Methods Enzymol. 383 (2004) 318–351.
[52] A. Koslowski, N. Sreerama, R.W. Woody, in: N. Berova, K. Nakanishi, R. Woody (Eds.), Theoretical approach to electronic optical activity in circular dichroism - principles and applications, Wiley-VCH, New York, 2000, pp. 55–95.
[53] T. Lu, F. Chen, Multiwfn: a multifunctional wavefunction analyzer, J. Comput. Chem. 33 (2012) 580–592.